Journal of Hydrology 626 (2023) 130289

Contents lists available at ScienceDirect

Journal of Hydrology

journal homepage: www.elsevier.com/locate/jhydrol

Research papers

Seawater intrusion assessment along the Volturno River (Italy) via numerical modeling and spectral analysis

Mattia Gaiolini [a], Nicolò Colombani [a], Micòl Mastrocicco [b], Matteo Postacchini [c,*]

[a] Department of Materials, Environmental Sciences and Urban Planning (SIMAU), Polytechnic University of Marche, 60131, Ancona, Italy
[b] Department of Environmental, Biological and Pharmaceutical Sciences and Technologies (DISTABIF), University of Campania "Luigi Vanvitelli", Via Vivaldi 43 81100, Caserta, Italy
[c] Department of Civil and Building Engineering, and Architecture (DICEA), Polytechnic University of Marche, 60131, Ancona, Italy

ARTICLE INFO

This manuscript was handled by Sally Elizabeth Thompson, Editor-in-Chief, with the assistance of Iryna Dronova, Associate Editor

Keywords:
Seawater intrusion
Numerical modeling
Tidal forcing
Remote sensing

ABSTRACT

Surface and groundwater salinization are becoming a significant challenge to inland water quality, negatively affecting people and ecosystems in coastal areas. Even if rivers provide critical pathways for seawater intrusion, this salinization phenomenon has received relatively little attention compared to other salinization mechanisms. To assess the distribution of salinity along the final reach of the Volturno River (Italy), an entire hydrologic year was modeled using the HEC-RAS software. The model was fed with high resolution time-series measurements (time interval of 10 min) of water surface elevations at both river mouth and Cancello Arnone (a hydrometric station located 13 km inland). Field observations and remote sensed data were used to perform the hydrodynamic analysis. The model showed good performance indicators ($R^2 = 0.878$, NSE = 0.870, and MAE = 0.037 m) and well caught hydrometric variation over the simulation period. The tidal component was affected by dissipation moving upstream and showed the capability to shape the salinity profile during dry periods. Whereas during wet periods, even if a strong tidal component is present, the profile is totally regulated by the river discharge. The analysis of the salinity distribution, modelled via the Water Quality module, revealed the massive contribution of the river discharge in limiting seawater intrusion. A correlation between intrusion events and hydrometric stages was established over twenty years (2002–2022), showing a consistent trend between intrusion occurrence and the surface water storage anomaly in the lower Volturno River calculated by Global Land Data Assimilation System (GLDAS) model. Although the 1D approach here used may lead to uncertainties in the reproduction of the involved hydrodynamic and salinization processes, the results are useful for the understanding of seawater intrusion in rivers, and may be utilized to study seawater intrusion in aquifers.

1. Introduction

Seawater intrusion (SWI) and more generally surface and groundwater salinization could negatively affect water quality and ecosystems in coastal areas all over the world (Klassen & Allen, 2017; Parizi et al., 2019; Cao et al., 2021; Mastrocicco & Colombani, 2021). Freshwater supplies' contamination (Werner et al., 2013), premature deterioration of co-existing infrastructure (Luo et al., 2015), eutrophication of surface water bodies (Weissman & Tully, 2020), soil salinization, and stress/death of salt-intolerant species including crops and forests (Kirwan & Gedan, 2019) are triggered by salinization, impacting people's health and livelihoods (Shammi et al., 2019). SWI may occur directly along coastal aquifers or via surface water bodies connected to the sea that provide critical pathways for seawater to travel upstream and salinize the adjacent groundwater body (Tully et al., 2019). As a matter of fact, surface- and ground-water interaction is considered to have significant effects on water resources salinization (Ferguson & Gleeson, 2012; Cao et al., 2020), although surface-water salinization has received relatively little attention compared to groundwater salinization mechanisms (Shalem et al., 2015; Shalem et al., 2019; Setiawan et al., 2023). The salinity distribution along a river strongly depends on the geometry of an estuary, but also on the freshwater discharge that counteracts SWI, being it induced either by the long-distance upriver propagation of the main tidal constituents (Melito et al., 2020; Postacchini et al., 2020) or

* Corresponding author.
E-mail addresses: m.gaiolini@pm.univpm.it (M. Gaiolini), n.colombani@univpm.it (N. Colombani), micol.mastrocicco@unicampania.it (M. Mastrocicco), m.postacchini@staff.univpm.it (M. Postacchini).

https://doi.org/10.1016/j.jhydrol.2023.130289
Received 8 May 2023; Received in revised form 7 August 2023; Accepted 14 September 2023
Available online 6 October 2023

by the short distance traveled by the shorter wind/swell waves during sea storms, leading to strong river-sea interactions up to some hundreds of meters from the mouth (Ralston et al., 2008; Nguyen et al., 2012; Postacchini et al., 2023). Moreover, the interaction of tides with river discharge directly affects SWI limiting freshwater availability (Hoitink & Jay, 2016; Savenije, 2012). In estuaries, it is notoriously hard to estimate this discharge and subsequently to predict the parameters that determine the mixing behavior depending on it (Cai et al., 2015). Thus, the spectral distribution analysis of water-levels at selected river cross-sections may be relevant to elucidate tidal propagation inland (Zhang et al., 2018; Postacchini et al., 2020).

In the last decades numerical modeling has been widely used to manage water resources allowing the organization of many available information (Loucks & van Beek, 2017). Water quality modeling is increasingly recognized as a fundamental tool for acquiring valuable information for optimal water resources management (Fan et al., 2009). Over the years, several water quality models have been developed using different software (Rauch et al., 1998), including basic water quality indices and user-friendly approaches (Wang et al., 2005; Haddout et al., 2017), but even more complex water quality criteria and methods (Reichert et al., 2001; Pelletier et al., 2006; Tung & Yaseen, 2020). Complex simulation models can involve multiple parameters, often not measured or reported, requiring abundant monitoring data for the estimation, calibration, and verification of model parameters. Hence, the use of complex models for water quality simulation could be difficult (Lindenschmidt, 2006) and limited to highly monitored sites. While simplified one-dimensional (1D) approaches have been often applied to model water flow and water quality both in rivers and lakes (Doulgeris et al., 2012; Ahmed, 2014; Haque et al., 2021; Thanh et al., 2023; Miller, 2023). Even if this approach simplifies the complex interactions involved in the river salinization process, it allows for efficient and robust simulation, making it feasible to analyze extensive high-resolution time series data (time interval of 10 min) and providing valuable insights into the salinization dynamics while balancing the computational complexity and data requirement. Few studies used HEC-RAS to quantify SWI along rivers so far (Haddout et al., 2017; Ijaz et al., 2019; da Silva et al., 2020), while the majority employed it to pursuit other objectives, often coupling it with other computer programs (Tamiru & Dinka, 2021; Muñoz et al., 2022; Postacchini et al., 2022). Since SWI will likely be exacerbated by climate change projections of sea level rise, increased frequency and intensity of sea storms, tides and reduced river flows (Anderson & Lockaby, 2012; Tully et al., 2019), the combined modeling and spectral analysis here proposed is crucial for an optimal management of estuarine and coastal areas (Demirel, 2004) providing valuable understandings of the river salinization dynamics.

Following this rationale, this study aims to assess the salinization dynamics along the Volturno River (Southern Italy) performing: i) a 1D hydrodynamic model to evaluate the hydraulic regime over the hydrologic year, ii) a spectral analysis to infer sea-river interactions and up-river tide propagation, and iii) a 1D water quality model to estimate the salinity concentration distribution along the river and to find a relationship between SWI events and critical hydrometric stages over 20 years (2002–2022).

To the best of our knowledge, there are no studies in literature combining 1D HEC-RAS modeling and spectral analysis to study river salinization mechanisms, especially considering an entire hydrologic year.

2. Materials and methods

2.1. Study area and model set up

The Volturno River is the sixth-longest river in Italy and the longest in Southern Italy, with a length of 175 km and an estimated mean discharge of 43 m^3s^{-1} for the period 2011–2040 (Copernicus, 2023). The catchment basin of the river has an area of ~5,550 km^2, crossing a huge area of the Campania region. The temperate and pleasant climate made this territory famous and renowned also for the woods and the extraordinary landscape with historical, cultural, and agricultural traditions unique in the world. Today, as it has been in the past, significant agricultural activity continues to thrive in this region, making it one of the primary pillars of the Campania region's economy (Triassi et al., 2022). The last reach of the river is characterized as sandy natural stream, while the prosper agricultural tradition enriches the river floodplain with vegetation and cultivated area at the overbanks.

Precipitation, hydrometric levels, and other parameters are continuously monitored by the Centro Funzionale Multirischi (2023) of the Civil Protection Agency of the Campania Region along the course of the river. This work focuses only on the last reach of the river (Fig. 1) starting at Cancello Arnone (CA) river gauge and ending at the mouth of the river (~13 km). To retrieve topographic information and represent the Volturno alluvial plain morphology, a digital terrain model (DTM) with spatial resolution of 2x2 m cells was used (Busico et al., 2021). Projections relative to the EPSG: 32,633 coordinate system were fixed in GIS environment and the merged DTM was imported in RAS-Mapper interface. The HEC-RAS efficiency of model analysis and refinement was increased by granting the use and visualization of geospatial data (Ackerman et al., 2010), allowing to exploit national open online datasets to set up the model. The model geometry was built up sketching the final reach of the river, together with the left and right overbanks and cross sections in RAS-Mapper environment (Fig. 1).

Actual cross-sections retrieved from the local basin authority in.dwg format were processed in GIS environment and imported in RAS-Mapper as shapefiles. Levees were placed on topographical elevations according to the DTM and the Google Earth 2014 view. Bridges have been added into the model questioning Google Earth 2014 view for the bridge deck width and for the number and dimension of piers. In the bridge modeling, a value of 1.2 and 0.95 was assigned to drag and pier shape coefficients (HEC, 2022), respectively, accounting for the circular shape of the bridge piers. Finally, the contraction/expansion coefficients have been set in both the upstream and the downstream sections of all the bridges by accounting for a value of 0.3 and 0.5, respectively, as suggested in HEC (2022). These coefficients are particularly important if bridges are present since the bridge piers influence the flow motion at both upstream and downstream locations.

2.2. Hydrodynamic analysis

Salinity distribution is influenced by the hydrodynamic regime, which in turn highly depends on the river morphology (Haddout et al., 2017). Thus, the hydrodynamic regime was first studied performing a 1D unsteady flow simulation. In the hydrodynamics module, HEC-RAS solves the following 1D equations of continuity and momentum (Brunner, 2010):

$$\frac{\partial Q}{\partial x}+\frac{\partial A}{\partial t}-q_l=0, \tag{1}$$

$$\frac{\partial Q}{\partial t}+\frac{\partial (q2/a)}{\partial x}+gA\frac{\partial h}{\partial x}=gA\left\{\left[\frac{nQ}{AR2/3}\right]^2-\beta_0\right\} \tag{2}$$

where Q is the discharge; A is the cross-sectional area; x is the distance along the channel; t is time; q_l is the lateral inflow per unit of length; g is the acceleration of gravity; h is depth; β_0 is the bottom slope; n is the Manning's roughness coefficient; and R is the hydrodynamic radius. The Manning's roughness coefficient was spatially disaggregated into two values only, accounting for both the sandy natural channel and the vegetation and cultivated areas at the overbanks. This approach was used by many hydraulic modeling studies (Horritt and Bates, 2001; Aronica et al., 2002; Werner et al., 2005; Jung et al., 2012; Savage et al., 2016) and is broadly justified by Werner et al. (2005) who found that there is little benefit in applying spatially distributed roughness

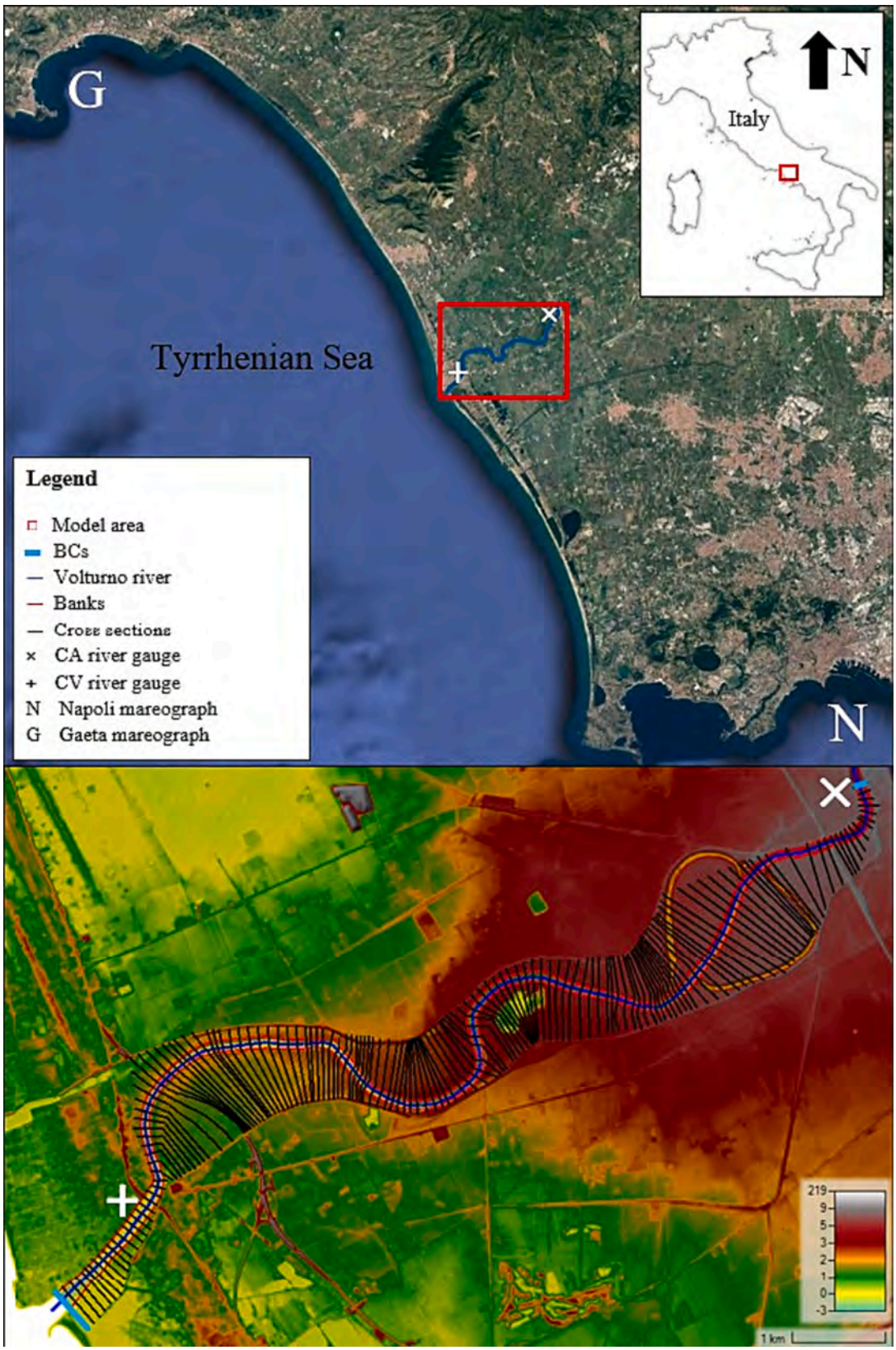

Fig. 1. Satellite view showing the main features of the study area (top panel) and RAS-Mapper view of the model area (bottom panel).

parameters.

The software requires the user to insert boundary conditions into the model and to specify the bridge modelling approach. Stage hydrograph boundary conditions were assigned to the most upstream (CA river gauge) and the most downstream (mouth of the river) cross-sections (Fig. 1), considering a temporal resolution of 10 min to infer tidal influence on river stage variation. Time series of Tyrrhenian Sea level data at Gaeta and Naples mareographs were downloaded from Servizio

Mareografico Nazionale (SMN) of the Istituto Superiore per la Protezione Ambientale (ISPRA), while river stages at both CA and Castel Volturno (CV) river gauges were downloaded from CFM.

For computing losses through the bridge, the energy-based method (standard step method) was selected, which treats a bridge in the same manner as a natural river cross-section, except that the area of the bridge below the water surface is subtracted from the total area, and the wetted perimeter is increased where the water is in contact with the bridge structure (HEC, 2022). The simulation plan was set to run the model for the entire hydrologic year (2014) selecting an output temporal resolution of 10 min, in accordance with the boundary conditions.

2.3. Spectral analysis

The hydrodynamic analysis outputs, together with the data collected by CA and CV river gauges and mareographs, were exploited to infer tidal propagation upriver and its relationship with SWI. A MATLAB code has been used to calculate the spectral density of both input and output data throughout the whole hydrologic year. In this way, the interactions occurring within the channel between tidal forcing and river discharge can be individuated, thus supporting the analysis of the distribution and propagation of the salinity concentration throughout the river (see section 2.4).

2.4. Water quality analysis

Modeling salinity evolution was achieved using the Water Quality module included in HEC-RAS, which is based on the 1D transport equation (advection–dispersion equation) of a conservative constituent (Brunner, 2010):

$$\frac{\partial(AC)}{\partial t}+\frac{\partial}{\partial x}(VAC)=\frac{\partial}{\partial x}\left[D_xA\frac{\partial C}{\partial x}\right] \quad (3)$$

where C is the salinity concentration; D_x is the longitudinal dispersion coefficient; V is the flow velocity. Velocity and water level were calculated earlier in the hydrodynamic analysis module, which is linked to the water quality module.

The salinity concentration was simulated as single parameter in the general constituent simulation module (GCSM), which requires the user to insert boundary and initial conditions values of salinity concentrations and the longitudinal dispersion coefficient (D) which in HEC-RAS is calculated by default using the Fischer's equation (Brunner, 2010):

$$D=0.011\frac{w^2v^2}{dv^*} \quad (5)$$

where v is the longitudinal velocity; w is the stream top width; d is the hydraulic depth; and v^* is the shear velocity.

A freshwater salinity concentration value of 0.4 g/L, based on the analysis of the historical major ions concentrations at the Capua measuring station (ARPAC, 2023) was assigned to the upstream boundary (CA) and a seawater salinity value of 38 g/L was assigned to the downstream boundary at the river mouth (Sorgente et al., 2020).

Values of $8x10^{-11}$ m^2/s and 50 m^2/s were assigned as lower and upper limits of D, which was computed using Eq. (5). The minimum value is representative of the sole molecular diffusion coefficient in water and the maximum value was sourced from Zheng & Huai (2014) that compiled a series of representative D values for rivers. Such an approach allowed for a longitudinal spatial distribution of the coefficient based on the hydrodynamic parameter's calculation at each cross-section. The simulation plan was set to run for the entire hydrologic year 2014 according to the unsteady flow simulation.

In addition, reasonable intrusion events at CA river gauge were investigated for an extended period (2002–2022), calculating the yearly SWI time occurrence as the percentage of days of the year during which a specified value of hydrometric stage is exceeded. To establish a correlation between SWI and hydrometric stages, three critical hydrometric stages (Hcrit) were identified through water quality analysis. These critical stages were the minimum Hcrit = -0.37 m addressing the initial transition from fresh to brackish water, the maximum Hcrit = -0.55 m indicating the point where the water became brackish, and the averaged Hcrit = -0.46 m calculated between the previous ones.

2.5. Remote sensing dataset and water quality dataset

To better characterize the SWI events and support the simulation, both remote sensing and water quality datasets were downloaded and compared with the water quality analysis results. The open-source web application called GRACE Groundwater Subsetting Tool (GGST) (McStraw et al., 2022) was interrogated to retrieve the surface water storage anomaly in the lower Volturno basin calculated by the GLDAS model (Rodell et al., 2004). GLDAS includes three separate land surface models: Noah, VIC, and CLSM, each of them producing an output for simulated surface water components (Rodell et al., 2004). The anomaly was computed subtracting the mean-centered on values from 2004 to 2009 and then averaging across the three GLDAS models to produce a component anomaly dataset. A time series was generated for the CA location, using the Marker Icon tool embedded in the GGST web application. Available precipitation data at CV and Grazzanise (located about 17 km inland) rain gauges were downloaded from CFM and the average monthly, seasonal, and yearly cumulated precipitation were calculated. The surface water quality database of the Environmental Protection Agency of Campania Region (ARPAC, 2023) was interrogated to retrieve electrical conductivity (EC) at 20 °C and dissolved chloride (Cl^-) monitored at CA from 2001 to 2020. Beside the ARPAC dataset, four additional EC data collected in 2014 during a large field campaign were retrieved from an internal database (Busico et al., 2018).

3. Results

3.1. Model performances and sensitivity analysis

The hydraulic model calibration was based on the comparison between simulated and measured water elevation at CV river gauge (Fig. 1), aimed at the optimal choice of Manning's roughness coefficient. Google Earth view together with literature values (Sturm, 2021) and field surveys were used to choose the appropriate coefficients fitting with both riverbed material and land cover. A further operation aimed at optimizing the software outputs was the correct selection of the channel bank stations and levees, for a suitable representation of the river flow dynamics. Best model performance indicators ($R^2 = 0.878$, NSE = 0.870, and MAE = 0.037 m) were retrieved considering values of the Manning's roughness coefficient of 0.03 and 0.1 for the channel and the overbank regions, respectively (Fig. 2a). Such values reflect the characteristics of the Volturno River accounting for the sandy natural stream, with vegetation and cultivated area at the overbanks (Sturm, 2021). The plotted stage hydrograph shows that the model well catches hydrometric variations due to both seasonal and tidal forcing along the river (Fig. 2b). To better highlight differences between wet and dry periods, a zoom in of both observed and calculated water levels was represented, selecting two different weeks within the simulated period (Fig. 2c and Fig. 2d).

A sensitivity analysis was performed to elucidate the uncertainties on Manning's roughness coefficient (Tab. 1).

A physically based range of values (Sturm, 2021) was used accounting for both the sandy natural channel (0.026—0.035) and the vegetation and cultivated areas at the overbanks (0.04—0.2). The results (Table 1) highlighted a very weak sensitivity of the parameter with negligible differences on all the model performance indicators with respect to the calibrated model.

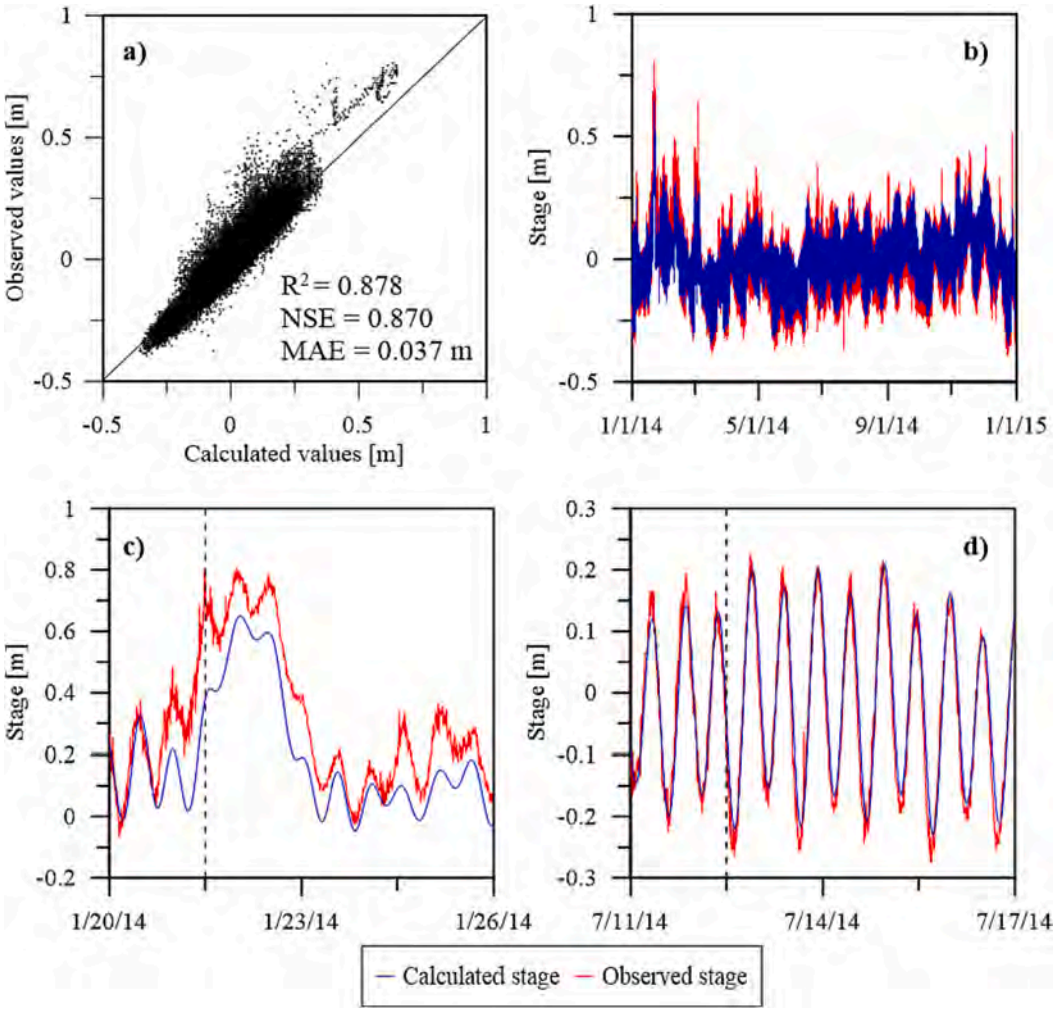

Fig. 2. Scatter Diagram (a) and comparison between HEC-RAS-calculated and CFM-observed river stages (b) with one week magnification for the wet and dry periods (c and d). Model performance indicators (R^2, NSE, and MAE) were calculated and represented in panel a. The vertical dashed lines refer to the instants selected for the salinity profile analysis, i.e., 21st of January at 00:00 and 12th of July at 00:00 (see section 3.3).

Table 1
Sensitivity analysis results of the physically based perturbation on Manning's roughness coefficient.

Manning's roughness coefficient		R^2	NSE	MAE [m]
Channel	Min 0.026	0.877	0.869	0.037
	Max 0.035	0.878	0.870	0.037
Floodplain	Min 0.04	0.877	0.869	0.037
	Max 0.2	0.878	0.869	0.037

3.2. Tidal forcing and spectral analysis

To better understand the role of marine forcing along the Volturno River, the water level signals at CA and CV river gauges together with the signal at the mouth of the river were filtered out of periods in the 12–24 h range. Then, the original and de-tided signals have been plotted together (Fig. 3a-c). The main outcome was that the tidal component could be considered negligible at CA (Fig. 3b), with the original and de-tided signals almost overlapping. Conversely, the tide played an important role at CV and at the mouth of the river (Fig. 3a and Fig. 3c). The dependence of each signal on the tidal constituents can be better seen in Fig. 3d and 3e, where the tidal component recorded at the mouth has been plotted against the same component recorded at CA and CV, for both the selected wet (Fig. 3e) and dry (Fig. 3f) periods. The data related to CV fall around the bisector, demonstrating a strong correlation with the tidal forcing, especially during the dry period (Fig. 3e). Conversely, the tidal component recorded at CA showed a weak dependence on the tidal forcing during both the analyzed periods. As the data slightly moved away from the bisector, the correlation with the tidal forcing at both CA and CV resulted to slightly decrease during the wet period, showing the capability of the Volturno River discharge to affect tidal propagation.

The role of the tide is better highlighted by the spatial distribution of the spectral density, which is illustrated in Fig. 4, for both wet and dry periods. Fig. 4a and Fig. 4c give a detailed overview and quantification of the spectral distribution at specific cross-sections, these being located either downstream (solid lines) or upstream (dashed lines) respect to CV. During both periods, spectral peaks appeared in correspondence with the semi-diurnal tidal constituent frequency ($f = 1/12$ Hz, rightmost black vertical lines), while a smoothed and lower peak appeared close to the diurnal constituent frequency ($f = 1/24$ Hz, leftmost black vertical lines). While the spectral density decreased rapidly after the semi-diurnal peak in the lower part of the river (solid lines), the farther cross-sections were characterized by a smoother decrease (dashed lines), indicating an energy redistribution over higher frequencies and a general reduction of the tide influence. The spatial evolution of the spectral energy is clearly visible in Fig. 4b and Fig. 4d where the macro-features during both periods are similar. In particular, the semi-diurnal constituent was strong enough to propagate up to CA and the spectral density related to higher frequencies increased moving upriver.

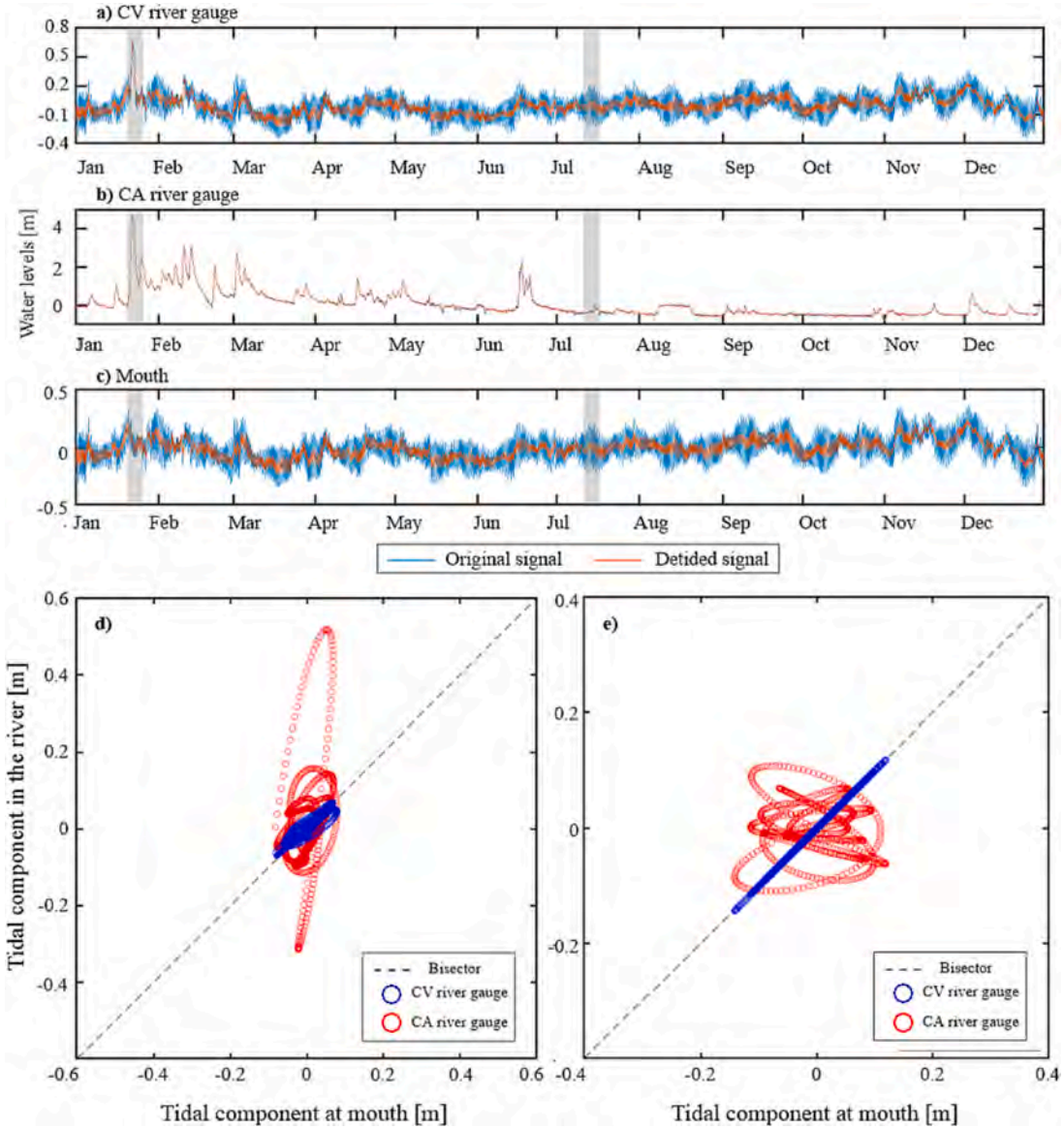

Fig. 3. Original (light blue) and de-tided (orange) signals recorded at **a)** the CV river gauge, **b)** the CA river gauge, and **c)** the mouth of the river; Scatter plots of the tidal component recorded at the mouth vs. those measured by CA (red circle) and CV river gauges (blue circle) for both the wet and the dry period (**d** and **e**, respectively), highlighted by the grey bands in panel **a**, **b**, and **c**. (For interpretation of the references to color in this figure legend, the reader is referred to the web version of this article.)

While the wet period was typified by a high spectral density at low frequencies (Fig. 4a) due to the low-frequency nature of floods, the dry period was more affected by the tidal intrusion, being the semi-diurnal peak (Fig. 4c) of an order of magnitude higher than that observed during the wet period (Fig. 4a). This was associated with the relatively low energy at low frequencies, being the floods almost inexistent (Fig. 4c). Furthermore, the frequency dispersion was much more evident during the wet period, being the spectral density at high frequencies ($f > 10^{-4}$ Hz) increased of about three orders of magnitude between the lower reach locations (e.g., at CV, shown by the solid black line) and the upper reach locations (e.g., at a distance from the mouth of 12.43 km, see the red dashed line). Such patterns are also illustrated in the color maps (Fig. 4b, Fig. 4c, and Fig. 4d), where the differences in the spatial evolution of the spectral density at different frequencies are clearly visible, especially at low frequencies ($f < 10^{-4}$ Hz) and at the semi-diurnal peak ($f \sim 2.3 \cdot 10^{-5}$ Hz).

3.3. SWI assessment

To graphically represent the salinity concentration distribution along the last reach of the river, HEC-RAS water quality spatial plot was questioned. Two snapshots within the wet and dry weeks (Fig. 2) were selected, to investigate SWI during both a high flow period (21st January 2014) and a low flow period (12th July 2014). The profiles were sketched in red, including the 6- and 12-hours after profiles (blue and green dashed lines) to infer tidal oscillation influence (Fig. 5). The salinity profile and schematic plot show the spatial distribution of the salinity concentration along the river to vary throughout the year, being affected by both tidal fluctuations and river discharge. During the selected low flow period, the salinity profile shows a periodic adaptation of the concentration at the mouth of the river according to the tidal oscillation (Fig. 5b). Such a behavior tends to reduce while moving upstream. During the high flow period, such oscillation cannot be detected (Fig. 5a) because of the dominance of the river discharge, which can be seen as the SWI controlling factor. A salinity concentration

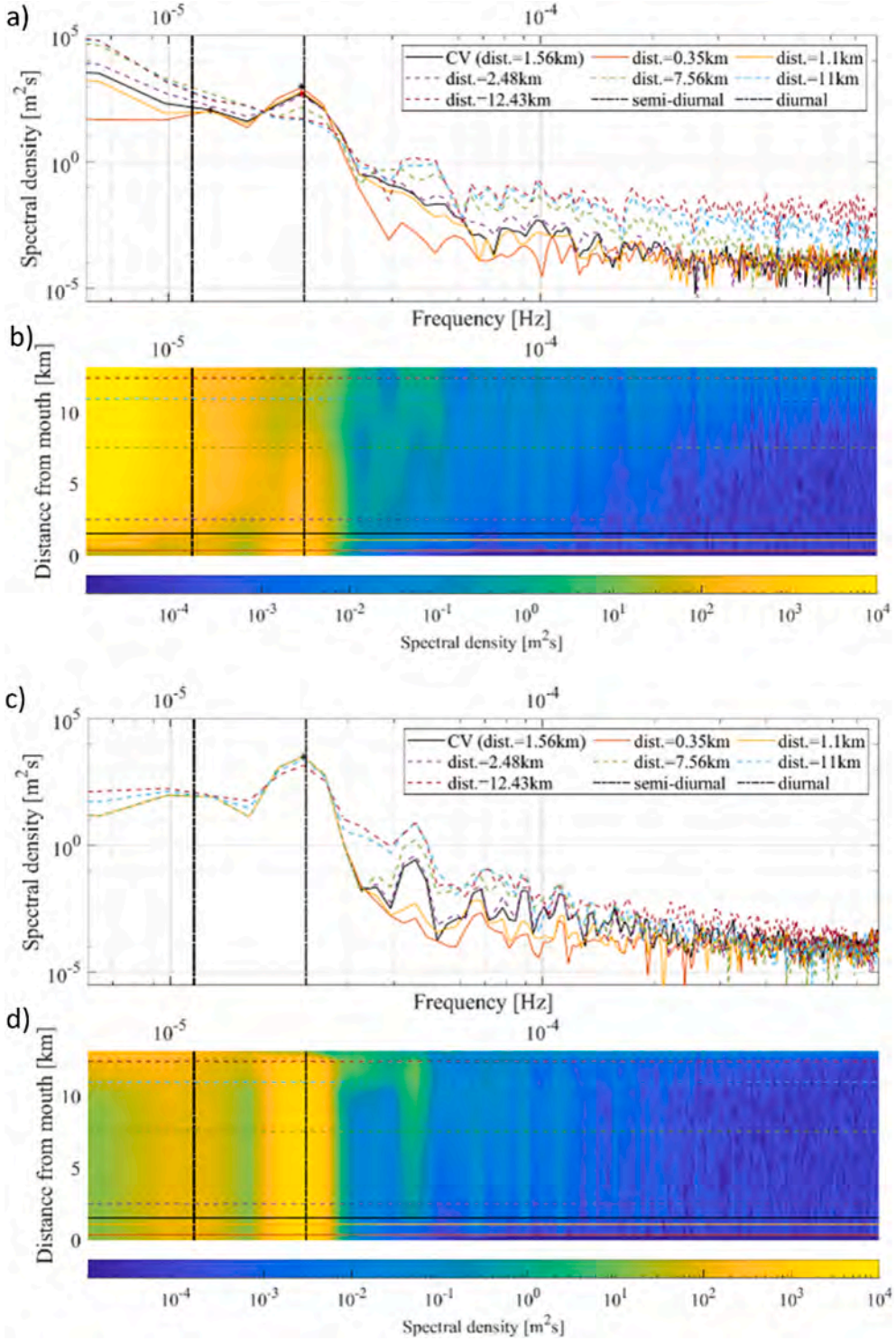

Fig. 4. Spectral density of the water level signals at selected cross-sections (**a**) and its spatial evolution from CA to the mouth (**b**) during the wet period, and for the dry period (**c** and **d**), as identified in Fig. 2. The vertical black lines show the frequency referring to the diurnal and semi-diurnal tidal constituents, while the horizontal lines in panels **b** and **d** indicate the location of the cross-sections used in panels **a** and **c**.

threshold of 5 g/L (dotted red line) was considered to map the SWI front moving upriver, accounting for the presence of brackish water into the river (Mayer et al., 2005). The water quality analysis clearly showed an advance of the seawater propagation front up to 2.2 km from the mouth during the high flow period, distance at which the salinity profile went below the concentration threshold line (Fig. 5a). During the low flow scenario, the salinity profile was always above the concentration threshold line (Fig. 5b), with concentration of almost 8 g/L at CA (~13 km inland).

The salinity concentration was plotted together with the river discharge at CA river gauge, where salinity concentration measurements were performed during 2014 (Fig. 6, upper panel). This analysis allowed an estimate of the pivotal contribution of the discharge to SWI. Accordingly, salinity concentration measurements in 2014 tend to rise when the river discharge is lower, as expected, thou their scarcity do not allow a proper validation of the model.

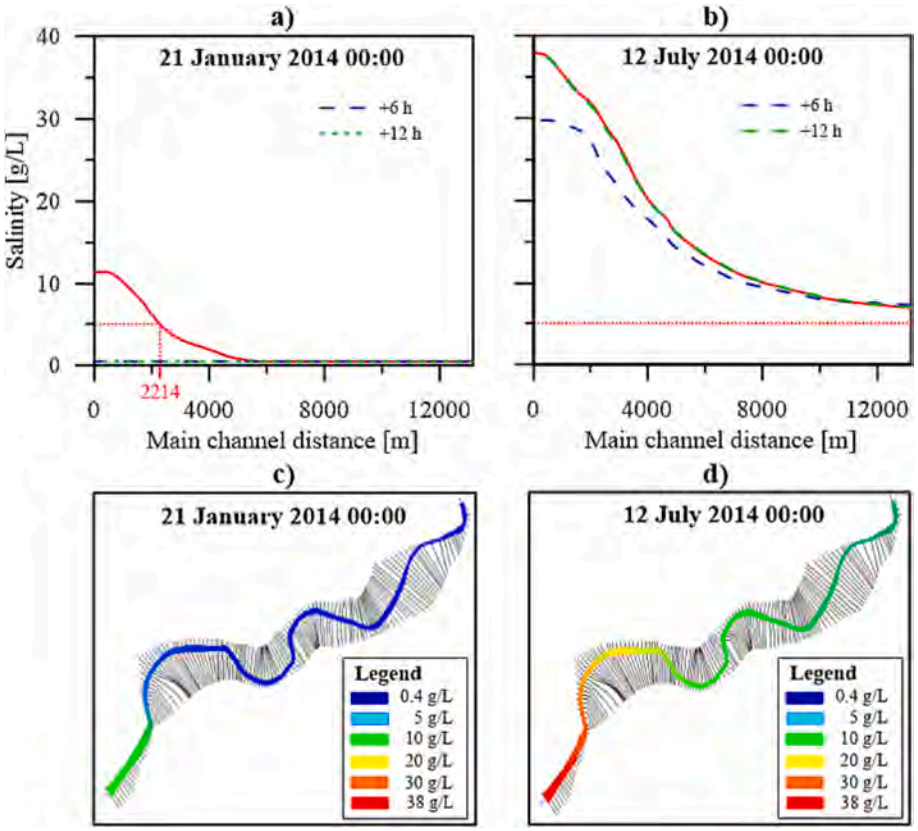

Fig. 5. Salinity profile and associated schematic plot snapshot for the 21st of January at 00:00 (**a** and **c**) and the 12th of July at 00:00 (**b** and **d**). The salinity profile after 6 h (blue dashed lines) and after 12 h (green dashed lines) are also shown (**a** and **b**) together with the considered salinity concentration threshold of 5 g/L (dotted red line). (For interpretation of the references to color in this figure legend, the reader is referred to the web version of this article.)

To further test the model results, Fig. 6 shows the GLDAS monthly surface water storage anomaly and its trend fitted via the locally estimated scatterplot smoothing (LOESS) algorithm. The latter is often used to infer trends from monthly and seasonal data (Apaydin et al., 2021). In the analyzed period, there was a decreasing trend of the GLDAS surface water storage anomaly, which was accompanied by the increase in EC and Cl^- concentration at CA.

With the aim of investigating reasonable intrusion events at CA river gauge for a longer period, yearly SWI time occurrence was calculated as the percentage of days of the year during which a specified value of hydrometric stage is exceeded. A correlation between SWI and hydrometric stages was established using 3 critical hydrometric stages (H_{crit}), and the CFM database was questioned again to download daily river levels from 2002 to 2022 at CA, which were compared to each H_{crit} to determine SWI time occurrence in each year (Fig. 7).

The upper and lower error bars represent the SWI yearly percentage of time calculated using maximum and minimum H_{crit}. Such analysis shows a persistent SWI occurrence within the analyzed period, with peaks in the dry years characterized by low surface water storage calculated by GLDAS. However, the yearly SWI time occurrence did not reveal a clear increasing or decreasing trend over the years. To explore the eventual correlation among precipitation, SWI time occurrence and GLDAS anomaly, the Pearson correlation coefficient at the monthly, seasonal, and yearly levels was calculated (Table 2). A slightly negative correlation with the SWI events, precipitation and GLDAS anomaly appears at the yearly time step with values of −0.64 and −0.65, respectively.

4. Discussion

The hydrodynamic analysis provides a good estimate of the river hydraulic regime over the simulation period yielding favorable results for the calibration process with physically based Manning's roughness coefficient values. However, it must be stressed that this study focused just on the final reach of the Volturno River not including the entire basin. Such a constraint leads the model to undervalue the runoff feeding the river during precipitation events and to a consequent underestimation of the hydrometric stage during wet periods up to about 20 cm (Fig. 2c). Conversely, the model is much more accurate during dry periods (Fig. 2d).

The investigation of marine forcing revealed that the tidal component was negligible at the CA river gauge, while significant at the CV and river mouth gauges (Fig. 3). The spectral analysis further shows a dissipation of the tidal effect moving upriver, linking it to its capacity of affecting the salinity profile calculated by HEC-RAS along the river during low flow periods (Fig. 5b). However, even if tides played an important role at CV during high flow periods, the salinity profile did not change along with tidal oscillations (Fig. 5a), highlighting the importance of Volturno River discharge in controlling SWI. Under such perspective, low flow conditions lead to an almost unchanged propagation of the tidal forcing up to CA, with small changes occurring at higher frequencies (Fig. 4c, d). Conversely, high flow conditions lead to a gradual reduction of the marine contribution (in particular the semi-diurnal tidal constituent), which becomes almost negligible at about 10 km from the mouth, and to a flow-energy redistribution towards higher frequencies (Fig. 4a, b). Such behavior agrees with what is typically observed in the sea, when short waves break over a submerged breakwater, the spectral density smooths and the energy is redistributed towards higher frequencies (Battjes & Beji, 1991). The interaction between tidal forcing and river discharge was instrumental in comprehending the distribution of salinity concentration across the river, as reported by Zhang et al. (2018).

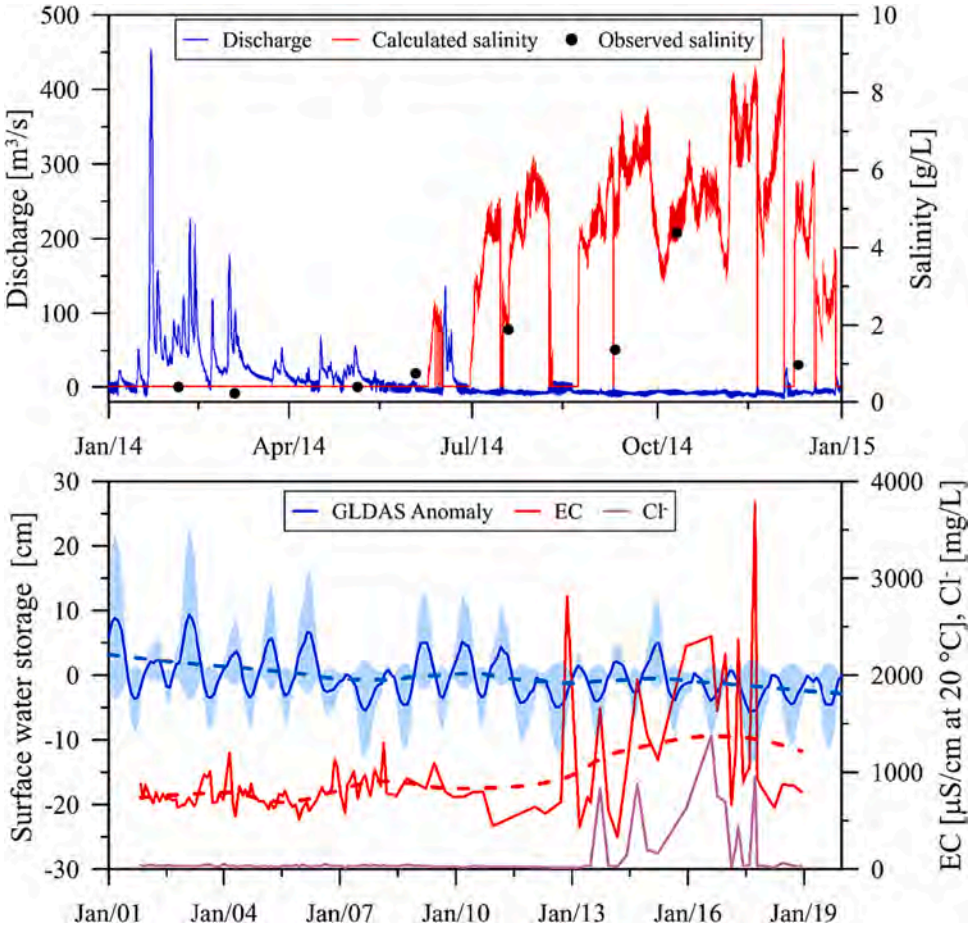

Fig. 6. In the upper panel, the calculated discharge (blue line), calculated salinity (red solid line) and observed salinity (black dots) are shown for the hydrological year 2014. In the lower panel, the GLDAS surface water storage anomaly (blue line) with its confidence interval (shaded blue area), the EC (red line) and Cl^- concentration (violet line) at CA are shown over 20 years (2001–2020). Dashed lines are the fitted GLDAS anomaly and the EC data trendline, according to the LOESS algorithm. (For interpretation of the references to color in this figure legend, the reader is referred to the web version of this article.)

The inverse correlation between SWI and Volturno River discharge (upper panel in Fig. 6) was also highlighted comparing yearly SWI time occurrence with both precipitation and GLDAS anomaly (Fig. 7). The correlation analysis at the yearly time step suggested an increase in SWI events in years with decreased precipitation and lower Volturno River discharge, in accordance with literature (Prandle, 2004; Brockway et al., 2006; Liu et al., 2007; Anderson & Lockaby, 2012). Such a comparison with remote sensing and water quality datasets independently supported the simulation results considering the scarcity of flow discharge data.

The fact that Cl^- concentrations mimic the EC trend could be considered a direct proof that SWI reached CA since 2012. This agrees with the decreased estimated mean discharge of 43 m^3s^{-1} for the period 2011–2040 (Copernicus, 2023), which halved respect to the historical discharge in the'70 s of 95 m^3s^{-1} (Greco, 2012). Moreover, it can be noticed that EC and Cl^- were almost constant at CA in the decade 2002–2012, while started to increase from 2013, as also highlighted by the LOESS algorithm; this could be linked to the GLDAS surface water storage anomaly that reached the tipping point of zero in 2012 as highlighted by the LOESS algorithm. Unfortunately, the monitoring program at CA was halted from 2019 and no other data are available from the ARPAC database to further corroborate the actual trend.

The yearly trend analysis highlighted that an increase of SWI was evident in years characterized by decreased precipitation and Volturno River discharge. This is a common feature often found in literature (Nguyen et al., 2012; Guerra-Chanis et al., 2019). A clearer negative correlation was advisable at the seasonal and monthly scale among SWI percentage and discharge, although the link was no longer evident for the precipitation events, that cannot be directly related to the SWI percentage occurrence. This could be explained by the fact that using seasonal and monthly precipitation data depicts the run-off contribution of the coastal area, which is contributing little to the Volturno River discharge (Greco, 2012); on the other hand, the yearly precipitation trend was more similar to the whole Volturno watershed, which in turn was the driver of the Volturno River discharge.

Hence, it must be emphasized that the Volturno River plain was studied predominantly to assess groundwater salinization processes (Mastrocicco et al., 2019; Busico et al., 2021; Schiavo et al., 2023) or to focus on groundwater quality due to pollution (Corniello and Ducci, 2014), while only few studies were focused on surface waters (Isidori et al., 2004; Sorgente et al., 2020) and no studies nor reports have so far estimated the salinity gradient along the Volturno River despite this is the largest river in Southern Italy. This is a rule rather than an exception in the whole Mediterranean area. Thus, a continuous measurement of physical–chemical parameters needs to be included within the monitoring network to better assess SWI spatial and temporal variations in rivers.

4.1. Limitations

While this study provides valuable insights on river salinization mechanism, it is essential to acknowledge limitations and uncertainties when interpreting the results.

The use of a 1D modeling approach inherently simplifies the representation of the complex interactions involved in the river salinization

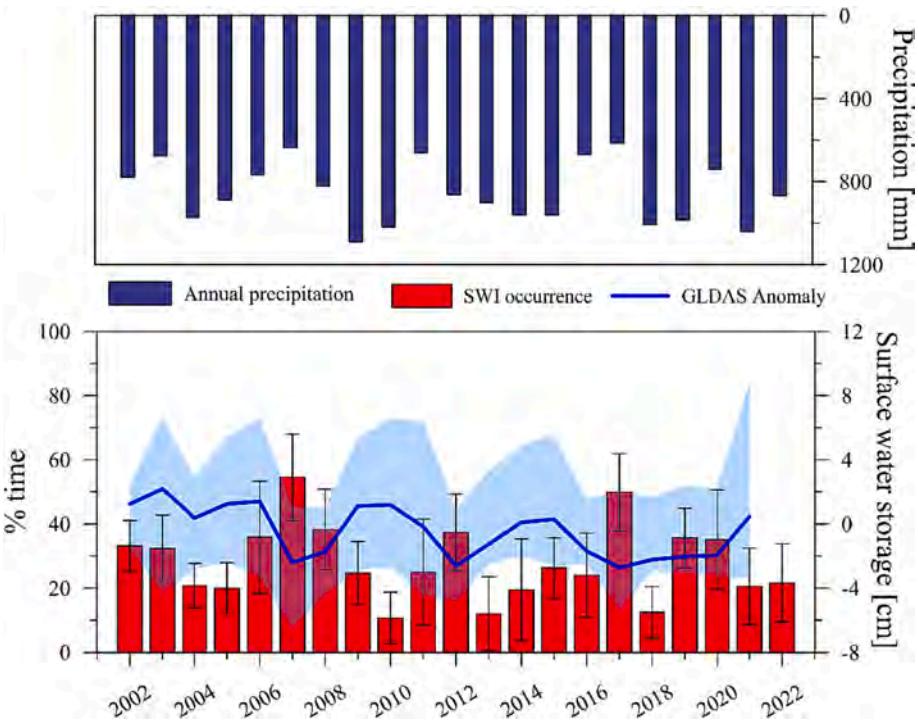

Fig. 7. Yearly cumulated precipitation from 2002 to 2022 (upper panel) and yearly SWI time occurrence according to the averaged H_{crit} (red bars), and surface water storage anomaly calculated by GLDAS (blue line and blue shaded area) (lower panel). The error bars show the SWI percentage of time in a year using the minimum and maximum H_{crit}. (For interpretation of the references to color in this figure legend, the reader is referred to the web version of this article.)

Table 2
Pearson coefficients for the SWI time occurrence and GLDAS anomaly and precipitation, using the yearly, seasonal, and monthly mean values.

SWI% Yearly mean		SWI% Seasonal mean		SWI% Monthly mean	
GLDAS	Precipitation	GLDAS	Precipitation	GLDAS	Precipitation
−0.649	−0.642	−0.767	−0.326	−0.721	−0.308

processes and may lead to some level of loss in capturing the full complexity of the phenomena under investigation.

The geometry of the cross-sections was assumed to remain constant throughout the simulations. This assumption might not fully account for potential changes in river morphology or bed configurations that could impact salinity distribution patterns.

The spatial disaggregation of the coefficient into two values for the channel and overbanks, while common in hydraulic modeling studies, might not capture localized variations in roughness conditions and their influence on the overall system behavior.

The water quality package integrated within the HEC-RAS software does not account for variable-density transport simulation. Therefore, the model's capability to accurately simulate salinity dynamics under varying densities induced by seawater intrusion and freshwater discharge, may be limited.

While these limitations need to be acknowledged, the study aims to provide a contribution to the understanding of SWI in rivers. By considering these constraints, researchers can better interpret the implications of the findings and identify areas for potential improvements in future studies. For example, if the aim is to use such results as input boundary conditions to feed complex density-dependent solute transport models (e.g., SEAWAT or FEFLOW) to study SWI in aquifers, the assumptions here made can be considered as valid given that the temporal resolution of groundwater models is usually at the monthly scale or larger and the spatial scale of aquifers are often very large.

5. Conclusions

A HEC-RAS 1D model was calibrated and validated to investigate the dynamics of SWI in the Volturno River. The calibrated model well catches the hydrometric variations due to tidal oscillations and seasonal changes over a whole hydrologic year. The SWI profile varied throughout the year, being affected by both tidal fluctuations and river discharge, with an advance of the SWI front up to 2.2 km during the high flow period and to more than 13 km during the low flow period.

A strong and an absent correlation with the tidal component was revealed at CV and CA, respectively. Moreover, the profile showed a strong salinity dependency on the tidal oscillation during low flow periods. While during wet periods, that oscillation cannot be detected because of the dominance of the river discharge as SWI controlling factor.

The correlation between SWI and critical hydrometric stages, found via modelling, allowed a better understanding of the SWI occurrence at CA over twenty years (2002–2022). Such analysis showed a persistent SWI occurrence within the analyzed period, with peaks in the dry years characterized by low surface water storage calculated by GLDAS.

The proposed modelling framework to retrieve key parameters (e.g., critical river water stages) and back calculating the SWI over longer times could be applied to similar coastal environments. As the SWI events would likely increase over time at the global scale, the proposed methodology could represent a useful tool to find simple relationships between widely monitored parameters (river water levels) and SWI and could serve as a starting point to define robust water resources management plans in coastal areas.

CRediT authorship contribution statement

Mattia Gaiolini: Conceptualization, Investigation, Methodology, Validation, Writing – original draft, Writing – review & editing. **Nicolò Colombani:** Conceptualization, Methodology, Supervision, Writing – review & editing. **Micòl Mastrocicco:** Conceptualization, Investigation,

Methodology, Writing – review & editing. **Matteo Postacchini:** Conceptualization, Methodology, Supervision, Writing – review & editing.

Declaration of Competing Interest

The authors declare that they have no known competing financial interests or personal relationships that could have appeared to influence the work reported in this paper.

Data availability

Data will be made available on request.

References

Ackerman, C.T., Jensen, M.R., Brunner, G.W. (2010). Geospatial capabilities of HEC-RAS for model development and mapping. In Proceedings of the 2nd Joint Federal Interagency Conference, Las Vegas, NV, USA (Vol. 27).

Ahmed, F., 2014. Cumulative hydrologic impact of wetland loss: numerical modeling study of the Rideau River Watershed, Canada. J. Hydrol. Eng. 19 (3), 593–606. https://doi.org/10.1061/(ASCE)HE.1943-5584.00008.

Anderson, C.J., Lockaby, B.G., 2012. Seasonal patterns of river connectivity and saltwater intrusion in tidal freshwater forested wetlands. River Res. Appl. 28 (7), 814–826. https://doi.org/10.1002/rra.1489.

Apaydin, H., Sattari, M.T., Falsafian, K., Prasad, R., 2021. Artificial intelligence modelling integrated with Singular Spectral analysis and Seasonal-Trend decomposition using Loess approaches for streamflow predictions. J. Hydrol. 600, 126506 https://doi.org/10.1016/j.jhydrol.2021.126506.

Aronica, G., Bates, P.D., Horritt, M.S., 2002. Assessing the uncertainty in distributed model predictions using observed binary pattern information within GLUE. Hydrol. Process. 16, 2001–2016. https://doi.org/10.1002/hyp.398.

ARPAC (2023). Online database on surface water quality of Campania Region. https://dati.arpacampania.it/dataset/monitoraggio-acque-superficiali-s07 Dataset identify number: arlpa:abdc59a2-71a2-4b39-aba8-d24a80d083a7 Last access at 13/03/2023.

Battjes, J.A., Beji, S. (1991). Spectral evolution in waves traveling over a shoal. Proceedings of the Nonlinear Water Waves Workshop, 11-19.

Brockway, R., Bowers, D., Huguane, A., Dove, V., Vessele, V., 2006. A note on salt intrusion in funnel-shaped estuaries: Application to the Incomati Estuary, Mozambique. Estuar. Coast. Shelf Sci. 66, 1–5. https://doi.org/10.1016/j.ecss.2005.07.014.

Brunner, G.W. (2010). HEC-RAS River Analysis System. Hydraulic Reference Manual. Version 4.1. U.S. Army Corps of Engineers, Hydrologic Engineering Center, Davis CA.

Busico, G., Cuoco, E., Kazakis, N., Colombani, N., Mastrocicco, M., Tedesco, D., Voudouris, K., 2018. Multivariate statistical analysis to characterize/discriminate between anthropogenic and geogenic trace elements occurrence in the Campania Plain, Southern Italy. Environ. Pollut. 234, 260–269. https://doi.org/10.1016/j.envpol.2017.11.053.

Busico, G., Buffardi, C., Ntona, M.M., Vigliotti, M., Colombani, N., Mastrocicco, M., Ruberti, D., 2021. Actual and forecasted vulnerability assessment to seawater intrusion via GALDIT-SUSI in the Volturno river mouth (Italy). Remote Sens. (Basel) 13 (18), 3632. https://doi.org/10.3390/rs13183632.

Cai, H., Savenije, H.H., Zuo, S., Jiang, C., Chua, V.P., 2015. A predictive model for salt intrusion in estuaries applied to the Yangtze estuary. J. Hydrol. 529, 1336–1349. https://doi.org/10.1016/j.jhydrol.2015.08.050.

Cao, T., Han, D., Song, X., Trolle, D., 2020. Subsurface hydrological processes and groundwater residence time in a coastal alluvium aquifer: evidence from environmental tracers ($\delta^{18}O$, $\delta^{2}H$, CFCs, ^{3}H) combined with hydrochemistry. Sci. Total Environ. 743, 140684 https://doi.org/10.1016/j.scitotenv.2020.140684.

Cao, T., Han, D., Song, X., 2021. Past, present, and future of global seawater intrusion research: A bibliometric analysis. J. Hydrol. 603, 126844 https://doi.org/10.1016/j.jhydrol.2021.126844.

Copernicus (2023). European hydrology and climate data explorer. https://cds.climate.copernicus.eu/cdsapp#!/software/app-hydrology-climate-explorer?tab=app.

Corniello, A., Ducci, D., 2014. Hydrogeochemical characterization of the main aquifer of the "Litorale Domizio-Agro Aversano NIPS" (Campania—southern Italy). J. Geochem. Explor. 137, 1–10. https://doi.org/10.1016/j.gexplo.2013.10.016.

da Silva, F.P., Martins, J.R.S., Nogueira, F.F., 2020. Impacts of sea level rise on seawater intrusion in Cubatão River, Brazil. Environ. Model. Assess. 25 (6), 831–841. https://doi.org/10.1007/s10666-020-09720-y.

Demirel, Z., 2004. The history and evaluation of saltwater intrusion into a coastal aquifer in Mersin, Turkey. J. Environ. Manage. 70, 275–282. https://doi.org/10.1016/j.jenvman.2003.12.007.

Doulgeris, C., Georgiou, P., Papadimos, D., Papamichail, D., 2012. Ecosystem approach to water resources management using the MIKE 11 modeling system in the Strymonas River and Lake Kerkini. J. Environ. Manage. 94 (1), 132–143. https://doi.org/10.1016/j.jenvman.2011.06.023.

Fan, C., Ko, C.H., Wang, W.S., 2009. An innovative modeling approach using Qual2K and HEC-RAS integration to assess the impact of tidal effect on River Water quality simulation. J. Environ. Manage. 90 (5), 1824–1832. https://doi.org/10.1016/j.jenvman.2008.11.011.

Ferguson, G., Gleeson, T., 2012. Vulnerability of coastal aquifers to groundwater use and climate change. Nat. Clim. Chang. 2 (5), 342–345. https://doi.org/10.1038/nclimate1413.

Greco, R., 2012. A fuzzy-autoregressive model of daily river flows. Comput. Geosci. 43, 17–23. https://doi.org/10.1016/j.cageo.2012.02.031.

Guerra-Chanis, G.E., Reyes-Merlo, M.Á., Díez-Minguito, M., Valle-Levinson, A., 2019. Saltwater intrusion in a subtropical estuary. Estuar. Coast. Shelf Sci. 217, 28–36. https://doi.org/10.1016/j.ecss.2018.10.016.

Haddout, S., Igouzal, M., Maslouhi, A., 2017. Modeling the effect of salt water intrusion in the Sebou River estuary (Morocco). Russ. Meteorol. Hydrol. 42 (12), 803–811. https://doi.org/10.3103/S1068373917120081.

Haque, A., Hossain, K.M.A., Shadia, N., 2021. Coupled 1D hydrodynamic-water quality model of Kobadak-Sibsa River system for salinity. Int. J. Environ. Sci. Dev. 12, 311–315. https://doi.org/10.18178/ijesd.2021.12.10.1355.

HEC (2022). HEC-RAS River Analysis System, User's Manual, Version 6.3, CPD-68, August 2022. Hydrologic Engineering Center, Institute for Water Resources, U.S. Corps of Engineers, Davis, CA.

Hoitink, A.J.F., Jay, D.A., 2016. Tidal river dynamics: Implications for deltas. Rev. Geophys. 54 (1), 240–272. https://doi.org/10.1002/2015RG000507.

Horritt, M.S., Bates, P.D., 2001. Predicting floodplain inundation: Raster-based modelling versus the finite-element approach. Hydrol. Process. 15, 825–842. https://doi.org/10.1002/hyp.188.

Ijaz, M.W., Mahar, R.B., Ansari, K., Siyal, A.A., 2019. Optimization of salinity intrusion control through freshwater and tidal inlet modifications for the Indus River Estuary. Estuar. Coast. Shelf Sci. 224, 51–61. https://doi.org/10.1016/j.ecss.2019.04.039.

Isidori, M., Lavorgna, M., Nardelli, A., Parrella, A., 2004. Integrated environmental assessment of Volturno river in South Italy. Sci. Total Environ. 327 (1–3), 123–134. https://doi.org/10.1016/j.scitotenv.2004.01.021.

Jung, H.C., Jasinski, M., Kim, J.W., Shum, C.K., Bates, P.B., Neal, J., Lee, H., Alsdorf, D., 2012. Calibration of two-dimensional floodplain modeling in the central Atchafalaya Basin Floodway System using SAR interferometry. Water Resour. Res. 48, W07511. https://doi.org/10.1029/2012WR011951.

Kirwan, M.L., Gedan, K.B., 2019. Sea-level driven land conversion and the formation of ghost forests. Nat. Clim. Chang. 9 (6), 450–457. https://doi.org/10.1038/s41558-019-0488-7.

Klassen, J., Allen, D.M., 2017. Assessing the risk of saltwater intrusion in coastal aquifers. J. Hydrol. 551, 730–745. https://doi.org/10.1016/j.jhydrol.2017.02.044.

Lindenschmidt, K.E., 2006. The effect of complexity on parameter sensitivity and model uncertain in river water quality modeling. Ecol. Model. 190, 72–86. https://doi.org/10.1016/j.ecolmodel.2005.04.016.

Liu, W., Chen, W., Cheng, R.T., Hsu, M., Kuo, A.Y., 2007. Modeling the influence of river discharge on salt intrusion and residual circulation in Danshuei River Estuary, Taiwan. Continental Shelf Res. 27, 900–921. https://doi.org/10.1016/j.csr.2006.12.005.

Loucks, D.P., van Beek, E., 2017. Water resources planning and management: An overview. In: Loucks, D.P., van Beek, E. (Eds.), Water Resource Systems Planning and Management. Springer International Publishing, Cham, pp. 1–49.

Luo, C.-Y., Shen, S.-L., Han, J., Ye, G.-L., Horpibulsuk, S., 2015. Hydrogeochemical environment of aquifer groundwater in Shanghai and potential hazards to underground infrastructures. Nat. Hazards 78 (1), 753–774. https://doi.org/10.1007/s11069-015-1727-5.

Mastrocicco, M., Busico, G., Colombani, N., Vigliotti, M., Ruberti, D., 2019. Modelling actual and future seawater intrusion in the Variconi coastal wetland (Italy) due to climate and landscape changes. Water 11 (7), 1502. https://doi.org/10.3390/w11071502.

Mastrocicco, M., Colombani, N., 2021. The Issue of groundwater salinization in coastal areas of the Mediterranean Region: A review. Water 13 (1), 90. https://doi.org/10.3390/w13010090.

Mayer, X., Ruprecht, J., Bari, M. (2005). Stream salinity status and trends in southwest Western Australia. Department of Environment, Salinity and land use impacts series, Report No. SLUI 38. ISBN:1-920947-25-6.

McStraw, T.C., Pulla, S.T., Jones, N.L., Williams, G.P., David, C.H., Nelson, J.E., Ames, D. P., 2022. An open-source web application for regional analysis of GRACE groundwater data and engaging stakeholders in groundwater management. J. Am. Water Resour. Assoc. 58 (6), 1002–1016. https://doi.org/10.1111/1752-1688.12968.

Melito, L., Postacchini, M., Sheremet, A., Calantoni, J., Zitti, G., Darvini, G., Penna, P., Brocchini, M., 2020. Hydrodynamics at a microtidal inlet: Analysis of propagation of the main wave components. Estuar. Coast. Shelf Sci. 235, 106603 https://doi.org/10.1016/j.ecss.2020.106603.

Miller, R.L., 2023. Forcing uncertainty and salinity response to dredging in a tidal freshwater river. Int. J. River Basin Manage. 21 (2), 243–251. https://doi.org/10.1080/15715124.2021.1961795.

Centro Funzionale Multirischi (CFM) Regione Campania Italy (2023). http://centrofunzionale.regione.campania.it/#/pages/dashboard Last access, 10/04/2023.

Muñoz, D.F., Yin, D., Bakhtyar, R., Moftakhari, H., Xue, Z., Mandli, K., Ferreira, C., 2022. Inter-model comparison of Delft3D-FM and 2D HEC-RAS for total water level prediction in coastal to inland transition zones. J. Am. Water Resour. Assoc. 58 (1), 34–49. https://doi.org/10.1111/1752-1688.12952.

Nguyen, D.H., Umeyama, M., Shintani, T., 2012. Importance of geometric characteristics for salinity distribution in convergent estuaries. J. Hydrol. 448, 1–13. https://doi.org/10.1016/j.jhydrol.2011.10.044.

Parizi, E., Hosseini, S.M., Ataie-Ashtiani, B., Simmons, C.T., 2019. Vulnerability mapping of coastal aquifers to seawater intrusion: review, development and application. J. Hydrol. 570, 555–573. https://doi.org/10.1016/j.jhydrol.2018.12.021.

Pelletier, G.J., Chapra, S.C., Tao, H., 2006. QUAL2Kw-a framework for modeling water quality in stream and rivers using a genetic algorithm for calibration. Environ. Model. Softw. 21, 419–425. https://doi.org/10.1016/j.envsoft.2005.07.002.

Postacchini, M., Darvini, G., Perugini, E., Martinelli, J., Ilari, M., & Brocchini, M. (2022). Upriver Propagation of Tidal Waves and Mouth Bar Influence at a Microtidal Estuary: Observations and Modeling. In *39th IAHR World Congress 2022: from Snow to Sea*. IAHR. 10.3850/IAHR-39WC2521711920221025.

Postacchini, M., Melito, L., Sheremet, A., Calantoni, J., Darvini, G., Corvaro, S., Memmola, F., Penna, P., Brocchini, M., 2020. Upstream propagating long-wave modes at a microtidal river mouth. Environ. Sci. Proc. 2 (1), 15. https://doi.org/10.3390/environsciproc2020002015.

Postacchini, M., Manning, A.J., Calantoni, J., Smith, J.P., Brocchini, M., 2023. A Storm Driven Turbidity Maximum in a Microtidal Estuary. Estuar. Coast. Shelf Sci. 288, 108350.

Prandle, D., 2004. Saline intrusion in partially mixed estuaries. Estuar. Coast. Shelf Sci. 59, 385–397. https://doi.org/10.1016/j.ecss.2003.10.001.

Ralston, D.K., Geyer, W.R., Lerczak, J.A., 2008. Subtidal salinity and velocity in the Hudson River estuary: Observations and modeling. J. Phys. Oceanogr. 38 (4), 753–770. https://doi.org/10.1175/2007JPO3808.1.

Rauch, W., Henze, M., Koncsos, L., Reichert, P., Shanahan, P., Somlyódy, L., Vanrolleghem, P., 1998. River water quality modelling: I. State of the art. Water Sci. Technol. 38 (11), 237–244. https://doi.org/10.1016/S0273-1223(98)00660-X.

Reichert, P., Borchardt, D., Henze, M., Rauch, W., Shanahan, P., Somlyódy, L., Vanrolleghem, P. (2001). River water quality model no. 1 (RWQM1): II. Biochemical process equations. Water science and Technology 43(5), 11-30. 10.2166/wst.2001.0241.

Rodell, M., Houser, P.R., Jambor, U.E.A., Gottschalck, J., Mitchell, K., Meng, C.J., Arsenault, K., Cosgrove, B., Radakovich, J., Bosilovich, M., Entin, J.K., Walker, J.P., Lohmann, D., Toll, D., 2004. The global land data assimilation system. Bull. Am. Meteorol. Soc. 85 (3), 381–394. https://doi.org/10.1175/BAMS-85-3-381.

Savage, J.T.S., Pianosi, F., Bates, P., Freer, J., Wagener, T., 2016. Quantifying the importance of spatial resolution and other factors through global sensitivity analysis of a flood inundation model. Water Resour. Res. 52 (11), 9146–9163. https://doi.org/10.1002/2015WR018198.

Savenije, H.H.G. (2012). Salinity and Tides in Alluvial Estuaries, 2nd ed. Elsevier, New York. 10.1016/B978-0-444-52107-1.X5000-X.

Schiavo, M., Colombani, N., Mastrocicco, M., 2023. Modeling stochastic saline groundwater occurrence in coastal aquifers. Water Res. 235, 119885.

Setiawan, I., Morgan, L.K., Doscher, C., 2023. Saltwater intrusion from an estuarine river: A field investigation. J. Hydrol. 617, 128955 https://doi.org/10.1016/j.jhydrol.2022.128955.

Shalem, Y., Weinstein, Y., Levi, E., Herut, B., Goldman, M., Yechieli, Y. (2015). The extent of aquifer salinization next to an estuarine river: an example from the eastern Mediterranean. Hydrogeology Journal 23(1), 69-79. 10.1007/s10040-014-1250 1192-3.

Shalem, Y., Yechieli, Y., Herut, B., Weinstein, Y., 2019. Aquifer response to estuarine stream dynamics. Water 11 (8), 1678. https://doi.org/10.3390/w11081678.

Shammi, M., Rahman, M.M., Bondad, S.E., Bodrud-Doza, M., 2019. Impacts of salinity intrusion in community health: a review of experiences on drinking water sodium from coastal areas of Bangladesh. Healthcare 7 (1). https://doi.org/10.3390/healthcare7010050.

Sorgente, R., Di Maio, A., Pessini, F., Ribotti, A., Bonomo, S., Perilli, A., Alberico, I., Lirer, F., Cascella, A., Ferraro, L., 2020. Impact of freshwater inflow from the Volturno river on coastal circulation. Front. Mar. Sci. 7, 293. https://doi.org/10.3389/fmars.2020.00293.

Sturm, T.W., 2021. Open channel hydraulics, 3rd ed. McGraw Hill, New York.

Tamiru, H., Dinka, M.O., 2021. Application of ANN and HEC-RAS model for flood inundation mapping in lower Baro Akobo River Basin, Ethiopia. J. Hydrol.: Reg. Stud. 36, 100855 https://doi.org/10.1016/j.ejrh.2021.100855.

Thanh, T. N., Huynh Van, H., Vo Minh, H., Tri, V. P. D. (2023). Salinity Intrusion Trends under the Impacts of Upstream Discharge and Sea Level Rise along the Co Chien River and Hau River in the Vietnamese Mekong Delta. Climate, 11(3), 66. 10.3390/cli11030066.

Triassi, M., Montuori, P., Provvisiero, D.P., De Rosa, E., Di Duca, F., Sarnacchiaro, P., Díez, S., 2022. Occurrence and spatial-temporal distribution of atrazine and its metabolites in the aquatic environment of the Volturno River estuary, southern Italy. Sci. Total Environ. 803, 149972 https://doi.org/10.1016/j.scitotenv.2021.149972.

Tully, K., Gedan, K., Epanchin-Niell, R., Strong, A., Bernhardt, E.S., BenDor, T., Mitchell, M., Kominoski, J., Jordan, T.E., Neubauer, S.C., Weston, N.B., 2019. The invisible flood: the chemistry, ecology, and social implications of coastal saltwater intrusion. Bioscience 69 (5), 368–378. https://doi.org/10.1093/biosci/biz027.

Tung, T.M., Yaseen, Z.M., 2020. A survey on river water quality modelling using artificial intelligence models: 2000–2020. J. Hydrol. 585, 124670 https://doi.org/10.1016/j.jhydrol.2020.124670.

Wang, X., Homer, M., Dyer, S.D., White-Hull, C., Du, C., 2005. A river water quality model integrated with a web-based geographic information system. J. Environ. Manage. 75 (3), 219–228. https://doi.org/10.1016/j.jenvman.2004.11.025.

Weissman, D.S., Tully, K.L., 2020. Saltwater intrusion affects nutrient concentrations in soil porewater and surface waters of coastal habitats. Ecosphere 11 (2), e03041. https://doi.org/10.1002/ecs2.3041.

Werner, A., Bakker, M., Post, V.E.A., Vandenbohede, A., Lu, C., Ataie-Ashtiani, B., Simmons, C.T., Barry, D.A., 2013. Seawater intrusion processes, investigation and management. Recent Adv. Future Challenges 51, 3–26. https://doi.org/10.1016/j.advwatres.2012.03.004.

Werner, M., Blazkova, S., Petr, J., 2005. Spatially distributed observations in constraining inundation modelling uncertainties. Hydrol. Process. 19, 3081–3096. https://doi.org/10.1002/hyp.5833.

Zeng, Y., Huai, W., 2014. Estimation of longitudinal dispersion coefficient in rivers. J. Hydro Environ. Res. 8, 2–8. https://doi.org/10.1016/J.JHER.2013.02.005.

Zhang, F., Sun, J., Lin, B., Huang, G., 2018. Seasonal hydrodynamic interactions between tidal waves and river flows in the Yangtze Estuary. J. Mar. Syst. 186, 17–28. https://doi.org/10.1016/j.jmarsys.2018.05.005.